

# Quantum Vertex Model for Reversible Classical Computing

C. Chamon,<sup>1,\*</sup> E. R. Mucciolo,<sup>2</sup> A. E. Ruckenstein,<sup>1</sup> and Z.-C. Yang<sup>1</sup>

<sup>1</sup>*Physics Department, Boston University, Boston, Massachusetts 02215, USA*

<sup>2</sup>*Department of Physics, University of Central Florida, Orlando, Florida 32816, USA*

(Dated: August 31, 2024)

We construct a planar vertex model that encodes the result of a universal reversible classical computation in its ground state. The approach involves Boolean variables (spins) placed on links of a two-dimensional lattice, with vertices representing logic gates. Large short-ranged interactions between at most two spins implement the operation of each gate. The lattice is anisotropic with one direction corresponding to “computational” time, and with transverse boundaries storing the computation’s input and output. While we show that the model displays no finite temperature phase transitions, independent of circuit, the computational complexity is encoded in the scaling of the relaxation rate into the ground state with the system size. The paper uses thermal annealing and a novel and more efficient heuristic “annealing with learning” to study various computational problems. To explore faster relaxation routes, we construct an explicit mapping of the vertex model into the Chimera architecture of the D-Wave machine, initiating a novel approach to reversible classical computation based on state-of-the-art implementations of quantum annealing.

## I. INTRODUCTION

Throughout the past few decades, problems of computer science have become subjects of intense interest to theoretical physicists as novel paradigms of complex systems that could benefit from theoretical approaches and insights inspired by statistical physics. These include neural networks, Boltzmann machines and deep learning, compressed sensing, satisfiability problems, and a host of other approaches to data mining and machine learning [1–4]. The interest in the constraints on computation and information processing placed by physical laws is even older and dates to work by Landauer and Bennett [5–7]. One of the holy grails at the interface between physics and computer science is the physical realization of a large-scale quantum computer in which the processing of information makes use of quantum-mechanical concepts such as superposition and entanglement [8, 9]. However, building a quantum computer remains a challenging task: while very powerful and universal, the notion of quantum computing requires maintaining coherence over the duration of the computation, and strategies devised to fight decoherence [10–14] require very stringent conditions that have not yet been fully met in practice.

This paper, which hopes to bring a new class of problems to the physics-computer science interface, introduces a two-dimensional (2D) representation of a generic reversible classical computation, the result of which is encoded in the ground state of a statistical mechanics vertex model with appropriate boundary conditions. The vertex model is defined in terms of Boolean variables (or spins degrees of freedom) placed on the bonds or links of an anisotropic 2D lattice with vertices representing logic gates. The corresponding gate constraints are implemented through short-ranged one- and two-body interactions involving the spins of the vertex (as we show, this

construction can be realized in physical programmable machines, such as the D-Wave machine [15]). One direction of the lattice represents “computational (rather than real) time”, as introduced by Feynman in the history representation of quantum computation [16], but here used for classical reversible circuits. The two boundaries of the lattice transverse to the “time” direction contain the input and output bits of the computation. It is important to stress that we are not limiting ourselves to forward computations with fixed inputs. More interesting are problems in which only partial information about both inputs and outputs is known. In that case, reaching the ground state requires flow of information both forwards and backwards across the lattice, processes that are naturally built into our approach.

The idea of encoding classical computation in the ground state of a many-body spin model was introduced earlier for irreversible computation in Ref. [17–19]. Here we focus on reversible rather than irreversible computation in order to address problems with both fixed-input and mixed-boundary conditions on inputs and outputs, as explained above. Mapping onto a regular 2D lattice as opposed to an arbitrary graph allows us to use intuitive ideas from equilibrium and non-equilibrium statistical mechanics, especially of classical and quantum phase transitions. Also, while in Ref. [18] an error correction scheme was required to implement fault tolerant computation, in our scheme accurate computation without error correction is possible below moderate temperatures that scale only as the inverse of the logarithm of the system size, a consequence of the exponential scaling of the static correlation length with inverse temperature (see below). Most importantly, our work emphasizes that the dynamics of relaxation to the ground state rather than the thermodynamics of the model is essential for understanding the implications and complexity of ground state computation.

Before launching into the main body of the paper, we would like to summarize our results and comment on

\* Corresponding author: [chamon@bu.edu](mailto:chamon@bu.edu)

their significance. First, we show through an exact calculation that, irrespective of the details of the classical computation, the thermodynamics of the corresponding lattice model with either open or fixed-input boundary conditions shows no phase transition down to zero temperature. In particular, the resulting thermodynamic behavior is that of a paramagnet. We argue that this thermodynamic behavior is a bulk property, and is unaffected by changes of boundary conditions.

The absence of a thermodynamical phase transition removes an obvious impediment to reaching the ground state of the vertex model. For instance, a suboptimal mapping from a computational problem into a physical system may place the solution within a glassy phase, even in the case of easy computational problems. The mapping of XORSAT (a problem in P) into a diluted  $p$ -spin model is such an example [20]. The fact that our vertex model is free of thermodynamic transitions does not mean that one can always reach the ground state easily. In this paper we will focus on problems with a unique solution encoded by a vertex model with a unique ground state. This is a problem in the complexity class UNIQUE-SAT, which under randomized reduction is as hard as SAT [21]. Hence, even in the absence of a thermodynamic transition finding the unique ground state of vertex models encoding problems with a single solution is a problem in NP-complete [22–24]. Of course, this statement does not mean that one cannot benefit from speed-ups allowed by either physics inspired heuristics or by special-purpose physical hardware, such as quantum annealers.

This paper focuses on the study of vertex-model representations of random circuits for which the complexity of the computation is reflected in the concentration of TOFFOLI gates, the length of the input and output boundaries  $L$ , and the depth of the circuit  $W$ . This highlights another important aspect of the physics-inspired perspective, namely the interest in “typical” and “average” behavior rather than in worst-case scenarios. More precisely, here we focus on typical problems, *i.e.*, problems randomly drawn from the  $5^{LW}$  possible classical computations encoded in vertex models with fixed  $L$  and  $W$ , and a given concentration of TOFFOLI gates. Furthermore, as motivated below, we concentrate on computational problems with a single solution – or problems for which one can discern among an  $\mathcal{O}(1)$  number of solutions with a small overhead – a class of problems that encompass factoring of semi-primes, an important and nontrivial example that we shall explore in a future publication.

As stressed above, the absence of a thermodynamic phase transition independent of circuit underscores the fact that it is not the thermodynamics but rather the dynamics that reflects the computational complexity of a specific problem. Indeed, this complexity is encoded in the behavior of the rate of relaxation to the ground state as a function of the size and depth of the computation. The simplest way of studying this behavior

is via thermal annealing [25] by using a ramp protocol,  $T(t) = K(1 - t/\tau)$ , to cool the system, starting from the scale  $K$  down to zero temperature, over a total time duration  $\tau$ . At any temperature  $T$  along the annealing path, the correlation length is  $\ell_T(\tau) \leq \ell_T(\tau \rightarrow \infty) = \xi_T$ , where  $\xi_T \sim e^{K/2T}$  is the thermal correlation length in the paramagnetic state, and  $K$  is a characteristic ferromagnetic interaction strength in our model. In thermal equilibrium all gate constraints defining the computational circuit would be satisfied once  $\xi_T$  reaches the depth of the computation,  $W$ . Notice that the exponential dependence of  $\xi_T$  on temperature implies that achieving the correct assignment of gates does not require very low temperatures on the scale of  $K$  since  $\xi_T \sim W$  already for temperatures below  $T \sim K/\ln W$ . However, reaching the solution to the computational problem is a dynamical process that cannot proceed to completion until the *dynamic correlation length* at the end of the annealing protocol,  $\ell(\tau) = \ell_{T=0}(\tau)$ , reaches  $W$ , allowing the input and output boundaries of the system that specify the computation to communicate. In this paper, we identify this dynamical correlation length and study its scaling behavior numerically.

Not surprisingly, thermal annealing is not the most efficient dynamical path for bringing a system to solution. For instance, computations that proceed from a fully specified input boundary reach solution when  $\ell(\tau) \sim W$ . However,  $\ell(\tau)$  grows slower than ballistically (*i.e.*, linearly in  $\tau$ ), and thus the time-to-solution derived from simple annealing does not scale linearly in  $W$ , as expected for forward computation. A more efficient approach is to use a “learning” protocol which involves repeated annealing procedures applied to a large number,  $N_R$ , of identical replicas of the system over periods of time  $\tau_a$ , during which the dynamical correlation length grows beyond a few layers of vertices. After each annealing interval  $\tau_a$ , a histogram of possible states is built for every gate in the system, and some of the vertices are assigned particular states provided that a majority of replicas greater than a cutoff agree on the assignment. Subsequent annealing protocols are only applied to the remaining “unpinned” gates, a process which is repeated  $n_s$  times, until all vertices in the system are fixed. As illustrated in Figure 7, this protocol initiates a finite strip of matched vertices input boundary, which provide the initial condition for the next annealing cycle, thus pushing the computation forward. The “annealing with learning” protocol requires  $n_s \sim W$  steps, leading to a time to solution  $\tau_s \sim n_s \tau_a$  that is linear in depth of the computation  $W$ , thus matching the scaling of deterministic forward computation.

For computations with “mixed boundary conditions” defined by partially fixing bits on both input and output boundaries, communication between the two boundaries is necessary but not sufficient for negotiating the solution. Whether implemented by traditional thermal annealing or by “annealing with learning”, we find that the evolution to solution is arrested for both cases of multiple or no solutions, as we exemplify in our numerical

studies. By contrast, for problems with a single solution the “annealing with learning” protocol provides an unencumbered path to solution, as illustrated in Figure 8. We note that, although UNIQUE-SAT and SAT problems are both in NP-complete, the behavior of “typical” UNIQUE-SAT examples drawn from random vertex models corroborates the physical intuition that solutions to problems with non-degenerate ground states are not slowed down by the competition among degenerate domains.

Finally, we note that reaching the ground state of the vertex model could be accelerated by replacing classical annealing with quantum annealing [26–29]. While approaching computational problems through quantum annealing is left for future investigations, the current paper includes the formal derivation of the quantum version of the statistical mechanics model of reversible classical computation. This provides the background for another novel result of the paper, namely the explicit mapping of our lattice model onto the Chimera architecture of the D-Wave machine, a development that points to the potential usefulness of the vertex model as a programming platform for special purpose quantum annealers.

The paper is organized as follows: All the elements of the mapping of universal reversible classical computations into a model of interacting tiles fully covering a two-dimensional planar surface are given in Sec. II A. Sec. II A 1 introduces the implementation of relevant logic gates based on local spin Hamiltonians; Sec. II A 2 discusses the “grout” interaction between adjacent tiles, which ensures that spins (bits) shared by neighboring tiles are locked to one another; Sec. II A 3 concludes the description of the mapping by discussing the boundary conditions which encode information associated with the inputs and outputs of the computation. Sec. II B derives the strong-coupling limit of the tile model in which the truth tables associated with each logic gate are satisfied exactly. This limit is used in Sec. II B 1 to derive a quantum vertex model on a two-dimensional square lattice, which defines the framework for most of our discussions of reversible classical computation. Section III describes results outlined in the introduction, namely: the thermodynamics (Sec. III A), dynamics of relaxation to the ground state (Sec. III B) via thermal annealing (Sec. III B 1), and the “annealing with learning” methodology (Sec. III B 2), where we contrast problems with only one solution and those with either multiple or no solutions. Section IV presents the embedding of the vertex model of classical computation into the Chimera architecture of the D-Wave machine. The paper closes with a summary and a discussion of open problems and future directions of investigation in Sec. V.

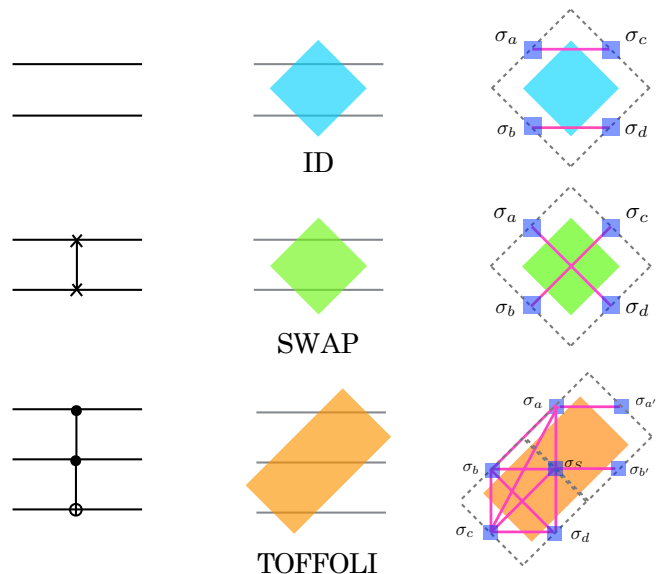


Figure 1. Elementary tiles representing the three computational gates for reversible circuits: ID (identity), SWAP and TOFFOLI. Right panel: construction of the Hamiltonians that encode the gate-satisfying states in the ground state manifolds. Spins are placed on the boundary of the tiles. For the TOFFOLI gate, an ancilla spin is placed in the center of the rectangular tile. Couplings needed in the Hamiltonians for the three different gates (tiles) are indicated by purple lines connecting two spins. The dashed line denotes the boundary of the tile.

## II. UNIVERSAL REVERSIBLE CLASSICAL COMPUTATION: THE MAPPING TO STATISTICAL MECHANICS MODELS

In this Section we formulate reversible classical computations by laying logic circuits in a two-dimensional structure of tiles covering the plane (Sec. II A) and discuss the vertex model, a more compact representation of the tile model (Sec. II B) that defines the context for the computational results of this paper.

### A. The Tile Model

Our starting point is the fact that any Boolean function can be implemented in terms of TOFFOLI gates, which are reversible logic gates with three inputs and three outputs. Starting from a circuit of TOFFOLI gates, our construction proceeds by first using SWAP gates to repeatedly swap distant bits in the input that are acted upon by particular gates of the circuit, until the operation of every gate is reduced to adjacent bits. The second step is to associate tiles with each of the gates, as shown in Fig. 1, where one should imagine placing input and output bits at the intersections of the tile surfaces with the horizontal lines, as will be described in detail shortly.

The tiles representing the gates can then be laid down

side-by-side in a plane to implement the computational circuit, as shown in Fig. 2 for the example of the “ripple-carry adder”, which computes the carry bit that is “rippled” to the next bit when adding two numbers [30]. (The “ripple-carry adder” is the building block for more complicated circuits such as addition and multiplication.) As can be seen from this example, one may also need to include the Identity (ID) gate in addition to the TOFFOLI and SWAP gates in order to represent particular logic circuits by a plane-filling tiling. Implied in the figure is that adjacent tiles share bits along common boundaries.

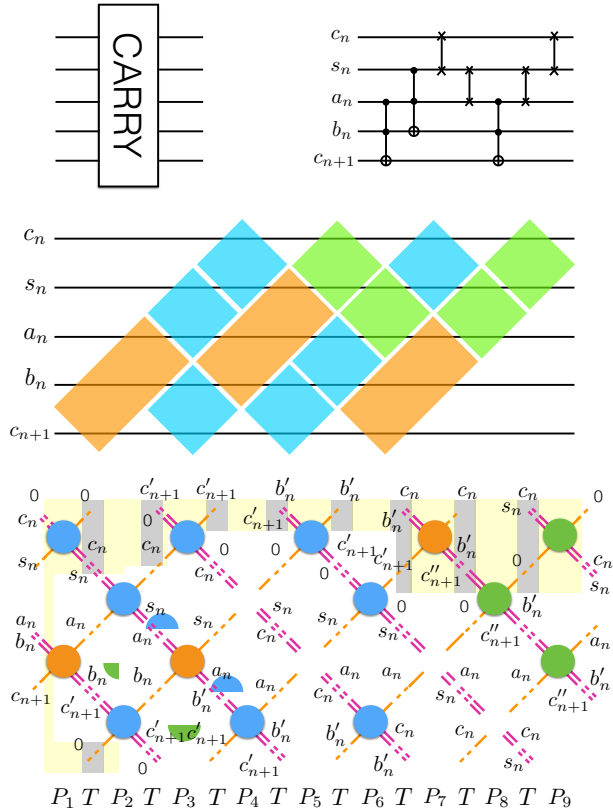


Figure 2. Upper panel: the ripple-carry adder which computes the carry bit that is “rippled” to the next bit. We add one additional control line  $s_n$  and set it to 1 to implement the original CNOT gate with a TOFFOLI gate. Middle panel: the ripple-carry adder implemented on the tile lattice, with different gates depicted in different colors: blue tile: ID; green tile: SWAP; gold tile: TOFFOLI. Spins between adjacent tiles are forced to be equal by the ferromagnetic ‘grout’ coupling  $K$ . Lower panel: the ripple-carry adder mapped to a vertex model with periodic boundary condition in the transverse direction. After each column of gate (vertex) operation, bit states are labeled at each bond. Light yellow and grey stripes represent the  $P$  and  $T$  matrices used in the transfer matrix calculation of the partition function.

We can now proceed with the explicit implementation of the general picture outlined above by constructing the Hamiltonian which encodes the solution of a computational problem in its ground state. The subsections below will set up the general framework and formulate approaches that form the basis of both the results of this paper and of work we are planning for the future.

### 1. Implementing Single Gate Operations by Spin-Hamiltonians with One- and Two-Body Interactions

We start by representing Boolean variables  $x_i = (1 + \sigma_i)/2$  in terms of spins  $\sigma_i = \pm 1$  placed on the boundary of each tile, as depicted in Fig 1. Operations of logic gates are then implemented in a similar way as in Ref. [17], by designing a Hamiltonian acting on the spins associated with individual tiles such that (a) the interactions are short ranged and involve at most two bodies; and (b) spin (i.e., bit) states that satisfy the gate constraint are ground states of the tile Hamiltonian and all other “unsatisfying” spin-states are pushed to high energies.

**Identity (ID) Gate:** The ID gate takes two bits  $(a, b)$  into  $(a, b)$ . This is easily enforced by adding ferromagnetic interactions ( $J > 0$ ) that align input bits  $a$  and  $b$  to output bits  $c$  and  $d$ , respectively, leading to an energy

$$E_{\text{ID}}(\sigma_a, \sigma_b; \sigma_c, \sigma_d) = -J(\sigma_a \sigma_c + \sigma_b \sigma_d). \quad (1)$$

**SWAP Gate:** The SWAP gate takes  $(a, b)$  into  $(b, a)$ , and can be implemented in the same manner as the ID gate through a ferromagnetic interaction ( $J > 0$ ),

$$E_{\text{SWAP}}(\sigma_a, \sigma_b; \sigma_c, \sigma_d) = -J(\sigma_a \sigma_d + \sigma_b \sigma_c). \quad (2)$$

**TOFFOLI Gate:** The TOFFOLI gate is represented by a rectangular tile with the three input bits  $(a, b, c)$  and three output bits  $(a', b', d)$  placed on the boundary, as shown in Fig. 1. Notice that in this case we also place an additional ancilla bit in the center of the rectangular tile, which is essential in order to satisfy the gate constraint with no more than two-body interactions. The TOFFOLI gate takes the three-bit input state  $(a, b, c)$  into  $(a, b, ab \oplus c)$ . The copying of the first two input bits from the input into the output is accomplished as before through a ferromagnetic coupling:  $-J(\sigma_a \sigma_{a'} + \sigma_b \sigma_{b'})$ . Enforcing the third output bit  $d = ab \oplus c$  requires a more involved interaction. We present the result below, and leave the detailed justification for the Supplementary Information. The complete energy cost associated to the TOFFOLI gate reads

$$\begin{aligned}
E_{\text{TOFFOLI}}(\sigma_a, \sigma_b, \sigma_c; \sigma_{a'}, \sigma_{b'}, \sigma_d; \sigma_S) = & -J(\sigma_a \sigma_{a'} + \sigma_b \sigma_{b'}) + J(\sigma_a - 3\sigma_b - 2\sigma_c + 2\sigma_d + 4\sigma_S) \\
& + J(-3\sigma_a \sigma_b - 2\sigma_a \sigma_c + 4\sigma_b \sigma_c + 2\sigma_a \sigma_d - 4\sigma_b \sigma_d - 4\sigma_c \sigma_d \\
& + 4\sigma_a \sigma_S - 8\sigma_b \sigma_S - 6\sigma_c \sigma_S + 6\sigma_d \sigma_S). \tag{3}
\end{aligned}$$

## 2. The global constraint and coupling of adjacent tiles

In addition to satisfying each gate separately, spins shared by neighboring tiles must be matched across the entire system in order for the tile model to accurately represent the desired computational circuit. To be precise one can imagine splitting each boundary spin into two ‘‘twin’’ spins and identifying input/output spins with each tile. Within this picture, adjacent spins at the boundary between tiles must be locked together, a constraint we implement by introducing a ferromagnetic ‘‘grout’’ coupling  $K > 0$  between spins on adjacent tiles. The corresponding term in the energy is then written as

$$E_{\text{grout}}(\{\sigma\}) = -K \sum_{\langle i,j \rangle} \sigma_i \sigma_j, \tag{4}$$

where  $\langle i, j \rangle$  labels pairs of ‘‘twin’’ spins  $i$  and  $j$  on the boundary between two adjacent tiles and the sum ranges over all such pairs of the system.

## 3. Boundary Conditions

Completing the description of the two-dimensional model of universal classical computation requires a discussion of boundary conditions, which determine the type of computational problem one is addressing. For example, if the  $N$ -bit input is fully specified and one is interested in the output, all that is needed is to transfer the information encoded into the input left to right by applying sequentially the gates one column of tiles at a time. In this case, if the depth (i.e., the number of steps) of the computation is a polynomial in  $N$ , this column-column computation reaches the output boundary, and thus solves the problem, in polynomial time.

As mentioned earlier, by using reversible gates one can also represent computational problems with mixed input-output boundary conditions for which only a fraction of the bits on the left (input) edge and a fraction of the bits on the right (output) edge are fixed. A concrete example is the integer factorization problem implemented in terms of a reversible integer multiplication circuit. A reversible circuit for multiplying two  $N$ -bit numbers  $p$  and  $q$  can be constructed using  $5N + 1$  bits in each column. One needs two  $N$ -bit registers for the two numbers  $p$  and  $q$  to be multiplied, one  $N$ -bit carry register  $c$  for the ripple-sums, a  $2N$ -bit register  $s$  for storing the answer  $p \times q = s$ , and one ancilla bit  $b$ . For multiplication, one only fixes the boundary conditions on the input:  $p$  and  $q$  are the two numbers to be multiplied, and  $c$ ,  $s$  and  $b$  are all 0's. For factorization we must impose mixed boundary

conditions: On the input side the  $c$ ,  $s$  and  $b$  registers are fixed to be all 0's; on the output side the  $s$  register is now fixed to the number to be factorized, and  $c$  and  $b$  are again all set to 0. Thus,  $3N + 1$  bits in the input and output are fixed, while  $2N$  bits are floating on both boundaries.

Boundary conditions on inputs, outputs, or both are imposed by inserting longitudinal fields at the appropriate bit sites, namely,

$$E_{\text{boundary}}(\{\sigma\}) = - \sum_{i \in \text{boundary}} h_i \sigma_i, \tag{5}$$

with  $|h_i| = h \gg J$ . The sign of an individual  $h_i$  field determines the value of the spin  $\sigma_i$  and thus of the binary variable  $x_i$ : For  $h_i > 0$ ,  $x_i = 1$ , while for  $h_i < 0$ ,  $x_i = 0$ . If no constraint is imposed on a binary variable  $x_i$ , then  $h_i = 0$ .

## B. The Vertex Model

The previous section led us to a classical Hamiltonian that includes the energy functions internal to each tile, the coupling between the spins at the boundary between adjacent tiles, and the magnetic fields associated with the input and output bits defining the boundary conditions of the computation, namely,

$$H_C = \sum_g E_g^J(\{\sigma\}_g) - K \sum_{\langle i,j \rangle} \sigma_i \sigma_j - \sum_{i \in \text{boundary}} h_i \sigma_i, \tag{6}$$

where  $\{\sigma\}_g$  labels all the spins and  $E_g^J(\{\sigma\}_g)$  represents the energy function of tile (i.e., gate)  $g$ .

This Hamiltonian is the starting point for our mapping of universal classical computation into the Chimera architecture of the D-Wave machine, one of the important results of the paper, which we discuss in Sec. IV. However, we find it more expedient and intuitive to work directly with tiles which satisfy the logic gate constraint exactly, a condition that can be realized in the limit of very large interaction  $J$  in Eqs. (1)-(3). In order to anticipate the fact that quantum rather than classical thermal annealing is the most effective way of reaching the ground state and therefore the solution of these computational problems, we add a transverse magnetic field  $\Gamma$  to Eq. (6) to obtain the quantum Hamiltonian

$$\begin{aligned}
\hat{H} = & \sum_g E_g^J(\{\hat{\sigma}^z\}_g) - K \sum_{\langle i,j \rangle} \hat{\sigma}_i^z \hat{\sigma}_j^z - \sum_{i \in \text{boundary}} h_i \hat{\sigma}_i^z \\
& + \Gamma \sum_i \hat{\sigma}_i^x. \tag{7}
\end{aligned}$$

We proceed by projecting the system onto the manifold of states where all local gate constraints are satisfied by working in the limit in which both  $h$  and  $J$  are very large; and we imagine varying  $K$  and  $\Gamma$ , with  $K, \Gamma \ll J, h$  [31]. This limit is best understood if we switch off the coupling between tiles,  $K$ . Within a given tile, the configurations that satisfy the logic gate constraints span the degenerate ground state manifold, while the unsatisfying configurations have energies of order  $J$  and higher. Let  $\{|q_a\rangle\}$ ,  $a = 1, \dots, r$  be all the  $r$  states spanned by the spin configurations  $|\sigma_1, \dots, \sigma_n\rangle$  that define the ground state manifold. For four-bit gates we have  $r = 4$ , while for six-bit gates  $r = 8$ .

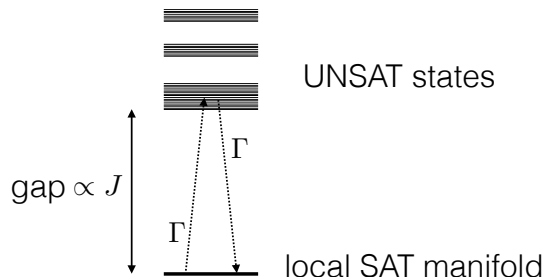


Figure 3. The limit  $J \gg K, \Gamma$  projects the spins onto the manifold of states that satisfy the local gate constraint. Transitions between the satisfying (SAT) configurations are possible via second-order processes involving virtual transitions onto the unsatisfying (UNSAT) states. The effective transition amplitude between the local SAT states is determined by  $\Delta = \Gamma^2/J$ .

As long as  $\Gamma \ll J$  we can understand the effect of a transverse field  $\Gamma$  on the  $r$  degenerate states by degenerate perturbation theory. Since for reversible gates maintaining the gate constraints requires at least two spin flips, the transverse field  $\Gamma$  induces an effective, second-order or higher spin-spin interaction on the ground state manifold of a given tile of order  $\Delta = \Gamma^2/J$  or lower. Figure 3 illustrates a second-order process.

Switching on the  $K$  coupling penalizes configurations in which the states of adjacent tiles are incompatible. Thus, in order to satisfy both intra- and inter-tile constraints that define the computational process we must reach the limit of  $\Delta \ll K \ll J, h$ .

### 1. The Quantum Vertex Model

To make the above discussion more concrete we derive an effective Hamiltonian of a quantum vertex model which allows us to investigate both the thermodynamics and dynamics of the system, and which we believe is the most effective formal setting for future work on the class of problems introduced in this paper.

For simplicity, we use rectangular tiles arranged so that all tiles have four neighbors (they are laid on a square lattice). We then combine pairs of ID and SWAP square tiles into four types of rectangular tiles, ID-ID, ID-SWAP,

SWAP-ID, and SWAP-SWAP. Any circuit can be laid down using these four rectangular tiles plus the TOF-FOLI tile. (The ripple-carry adder example in Sec. II A was not laid down in such way, but it can be easily rearranged into this form.)

Each tile, in the projected space of satisfying states, can be in one of  $r = 8$  states. We will place these 8-state variables at the vertices of a tilted square lattice, as shown in Fig. 2. The 8-state variable resides on the vertices of the lattice, and is indicated by the large dot. The links will contain the spin variables. There are six Boolean (or spin) variables associated to each vertex: two on each of the two double bonds and one in each of the two single bonds tied to each vertex. Three of the spins are inputs, and we use the state  $q$  of the vertex, where  $q = 0, 1, \dots, 7$ , to read-off the inputs in binary (which are uniquely related to the spin):  $x_a^{\text{IN}} = \text{bit}[a, q]$ ,  $a = 1, 2, 3$  for the three bits of the number  $q$ . The output bits are the bits of the 3-bit number  $G(q)$ , where  $G$  is the gate function:  $x_a^{\text{OUT}} = \text{bit}[a, G(q)]$ ,  $a = 1, 2, 3$ . The energy cost for two adjacent gates that are incompatible with each other is determined by the ferromagnetic coupling  $K$ .

One can express the Hamiltonian as

$$\begin{aligned} \hat{H} = & \sum_{\langle ss' \rangle} \sum_{q_s, q_{s'}} K_{q_s, q_{s'}}^{g_s, g_{s'}} |q_s q_{s'}\rangle \langle q_s q_{s'}| \\ & + \sum_{s \in \text{boundary}} \sum_{q_s} h_{q_s} |q_s\rangle \langle q_s| \\ & + \sum_s \sum_{q_s, q'_s} \Delta_{q_s, q'_s} |q_s\rangle \langle q'_s|, \end{aligned} \quad (8)$$

where  $K_{q_s, q_{s'}}^{g_s, g_{s'}}$  encodes the energy cost for mismatched nearest-neighbor vertices (the energies, with scale set by  $K$ , depend on the state of the vertices  $q_s$  and  $q_{s'}$ , as well as on the types of gates  $g_s$  and  $g_{s'}$  sitting at neighboring vertices  $s, s'$  – an explicit example is given in the supplementary material);  $h_{q_s}$  encodes the boundary conditions, which we associate directly with the vertex rather than with the input or output bits of a gate (since the relationship is one-to-one); and finally, the transition matrix elements  $\Delta_{q_s, q'_s}$  between the states within a vertex  $s$ . All these couplings can be determined given a computational circuit and the boundary conditions. The quantum term  $\Delta_{q_s, q'_s}$  can be designed from the internal couplings within the tiles; For simplicity, one should consider the case,  $\Delta_{q_s, q'_s} = \Delta$  for all  $q_s, q_{s'}$ , which then represents the 8-state counterpart of a transverse field.

The vertex model defined by Eq. (8) is the starting point for all the subsequent discussions of this paper. For example, a quantum annealing protocol for solving a factoring problem would start with  $K \ll \Delta$ , where the ground state is a superposition of all locally satisfied gates independent of one another, and end with  $K \gg \Delta$ , with a the ground state in which each tile satisfies the gate constraint and also passes and receives the right information to and from its neighbors.

### III. THERMODYNAMICS AND DYNAMICS OF THE CLASSICAL VERTEX MODEL

We are now in position to explore both the thermodynamics and the dynamics associated with the Hamiltonian in Eq. (8). The phase diagram of the model, as a function of both temperature and the quantum parameter  $\delta = \Delta/K$ , as well as the rate at which the system relaxes to the ground state give important information about the usefulness of the vertex model for solving classical computation problems.

$$Z = \sum_{\{\sigma_1\}, \dots, \{\sigma_{2W}\}} \langle \{\sigma_1\} | P_1 | \{\sigma_2\} \rangle \langle \{\sigma_2\} | T | \{\sigma_3\} \rangle \times \dots \times \langle \{\sigma_{2j-1}\} | P_j | \{\sigma_{2j}\} \rangle \langle \{\sigma_{2j}\} | T | \{\sigma_{2j+1}\} \rangle \times \dots \times \langle \{\sigma_{2W-1}\} | P_W | \{\sigma_{2W}\} \rangle, \quad (9)$$

where the matrix  $T$  encodes the energy costs for matching spins across the links, and the matrices  $P_j$  encode the computations performed by one column of gates. The two types of slices are depicted in Fig. 2. Notice that the  $T$  is the same for all slices, and its matrix elements are given by

$$\langle \{\sigma_{2j}\} | T | \{\sigma_{2j+1}\} \rangle = \exp \left( \sum_{a=1}^{3L} \beta K \sigma_{2j,a} \sigma_{2j+1,a} \right), \quad (10)$$

whereas  $\langle \{\sigma_{2j-1}\} | P_j | \{\sigma_{2j}\} \rangle$  represents the matrix element of  $P_j$  at the  $j$ th column and thus depends on the particular set of gates within that column. However, all  $P_j$  are permutation matrices since all gates are reversible. This fact is essential because it allows us to compute the partition function exactly, irrespective of the circuit.

For the next step notice that the vector  $|\Sigma\rangle = \sum_{\{\sigma\}} |\{\sigma\}\rangle$  is an eigenvector of  $P_j$  for any operation  $P_j$ :

$$P_j |\Sigma\rangle = P_j \sum_{\{\sigma\}} |\{\sigma\}\rangle = \sum_{\{\sigma\}} P_j |\{\sigma\}\rangle = \sum_{\{\sigma'\}} |\{\sigma'\}\rangle = |\Sigma\rangle, \quad (11)$$

where we used that we can relabel the states after the permutation. The vector  $|\Sigma\rangle = \sum_{\{\sigma\}} |\{\sigma\}\rangle$  is also an

#### A. Thermodynamics

We start by considering the partition function of the classical limit of the Hamiltonian in Eq. (8), i.e.,  $\Delta = 0$ , which we obtain via a transfer matrix calculation. Consider first a system with free boundary conditions at both ends. The partition function for the vertex model can be more easily written using the spin variables on the links of the lattice. Let  $\{\sigma\}_j$  denote the spin states on a vertical line, which cuts across  $3L$  spins (with  $L$  the number of vertices or 3-bit gates in a column). For convenience we shall utilize the notation  $|\{\sigma\}_j\rangle$  for the vectors in this transfer matrix calculation. Within this notation, one can write the partition function as

eigenvector of  $T$ :

$$\begin{aligned} T |\Sigma\rangle &= T \sum_{\{\sigma\}} |\{\sigma\}\rangle = \sum_{\{\sigma\}, \{\sigma'\}} |\{\sigma'\}\rangle \langle \{\sigma'\} | T | \{\sigma\} \rangle \\ &= \sum_{\{\sigma'\}} |\{\sigma'\}\rangle \sum_{\sigma} \exp \left( \sum_{a=1}^{3L} \beta K \sigma'_a \sigma_a \right) \\ &= \sum_{\{\sigma'\}} |\{\sigma'\}\rangle \prod_{a=1}^{3L} \sum_{\sigma_a = \pm 1} e^{\beta K \sigma'_a \sigma_a} \\ &= \sum_{\{\sigma'\}} |\{\sigma'\}\rangle (2 \cosh \beta K)^{3L} \\ &= (2 \cosh \beta K)^{3L} |\Sigma\rangle. \end{aligned} \quad (12)$$

By collecting all the factors we arrive at the partition function

$$Z = \langle \Sigma | P_1 T P_2 T \dots T P_W | \Sigma \rangle = (2 \cosh \beta K)^{3L(W-1)} \langle \Sigma | \Sigma \rangle. \quad (13)$$

The overlap  $\langle \Sigma | \Sigma \rangle = 2^{3L}$  reflects the  $2^{3L}$  degenerate ground states corresponding to open boundary conditions on both boundaries. Had we fixed one of the boundaries to a particular state  $|\{\sigma\}_{\text{fixed}}\rangle$  we would have instead obtained an overlap  $\langle \{\sigma\}_{\text{fixed}} | \Sigma \rangle = 1$ . More generally, in the thermodynamic limit boundaries contribute an entropic term that counts the number of ground states, but does not affect the bulk thermodynamics. In particular, the bulk free energy is that of a paramagnet:

$$\beta F = -[3L(W-1)] \ln(2 \cosh \beta K). \quad (14)$$

This also implies that thermodynamics alone, which is independent of the specific form of the circuit, cannot reveal the complexity of a ground-state computation, which is reflected in the dynamics of the system's relaxation into its ground state.

## B. Dynamics

In this section we study the dynamics of the vertex model using both traditional thermal annealing and a new “annealing with learning” algorithm.

### 1. “Vanilla” Annealing

Here we shall establish that the thermal annealing of the vertex model is controlled by a dynamical length scale  $\ell(\tau)$ , which grows with increasing times. In order to extract this length scale we study systems of different sizes, and collapse the data onto a single curve, following the dynamic scaling theory of Ref. [32] that builds on the Kibble-Zurek mechanism [33, 34]. Recently, this theory has been extended to include systems with zero-temperature order [35], the case relevant to the current discussion.

We start from a random vertex state  $\{q_s^{\text{initial}}\}$ , and lower the temperature from  $T = K$  to  $T = 0$  during a time interval  $\tau$ , according to the following protocol:

$$T(t) = K (1 - t/\tau) . \quad (15)$$

The scaling behavior is extracted by following an order parameter  $m$  that measures the overlap of the final state  $\{q_s^{\text{final}}\}$  reached at  $t = \tau$  with the reference (solution) state  $\{q_s^{\text{sol}}\}$ :

$$m = \frac{8}{7} \left[ \frac{1}{LW} \sum_s \delta_{q_s^{\text{final}}, q_s^{\text{sol}}} - \frac{1}{8} \right] . \quad (16)$$

(Below we explain in detail how a unique solution state  $\{q_s^{\text{sol}}\}$  is obtained.) Notice that the order parameter reaches  $m = 1$  when the final state agrees with the solution, and  $m = 0$  if the state is random, in which case it agrees with the solution by chance in 1/8th of the sites. We remark that the “solution overlap” is a much better indicator of the evolution towards solution than the total energy. This is because a single vertex flip into an incorrect state in the middle of the circuit may cost little energy but it throws other vertices into a completely different state from the correct one.

The numerical Metropolis simulations are carried out as follows. We work on a lattice of  $L \times W$  vertices, using the Hamiltonian of Eq. (8) with  $\Delta_{q_s, q'_s} = 0$ . Periodic boundary conditions are used in the transverse direction, i.e., the circuit is laid down on the surface of a tube of length  $W$  and circumference  $L$ . We consider four types of circuits corresponding to different concentrations of TOFFOLI gates (the other four types of gates are assigned equal concentrations): 1. all TOFFOLI gates; 2. random circuits with 40% of TOFFOLI gate; 3. random circuits with 20% of TOFFOLI gates; and 4. random circuits with no TOFFOLI gates. As we will see shortly, the concentration of TOFFOLI gates dictates the complexity of the computational problem, as all non-trivial operations between input and output bits involve TOFFOLI

gates. The first step of the simulation is to construct a reference state  $\{q_s^{\text{sol}}\}$  that solves the circuit, by fixing the states  $q_s^{\text{sol}}$  for the vertices  $s$  at the left boundary, and determining and storing all other states  $q_s^{\text{sol}}$  for vertices  $s$  in the rest of the circuit. Next, we construct three explicit boundary conditions consistent with the reference state,  $\{q_s^{\text{sol}}\}$ , that will serve as the input states for our simulations: 1. fixed input, for which we apply pinning fields at the left boundary that fix the states to match  $q_s^{\text{sol}}$  for the vertices  $s$  at the left boundary, and leave the other boundary free (no pinning field); 2. fixed input and output, for which we pin all vertices  $s$  on the left and right boundaries to those defined by  $q_s^{\text{sol}}$ ; and 3. mixed boundaries, for which we pin  $L_\partial = L/2 + 3$  vertices on both the left and right boundaries to the solution values  $q_s^{\text{sol}}$ , but leave all the remaining boundary vertices free. Our computations proceed in each of these three cases by averaging over 2000 independent random instances of input states for a given circuit with a fixed concentration of TOFFOLI gates corresponding to different  $\{q_s^{\text{sol}}\}$  and computing the average order parameter  $\langle m \rangle$  as a function of the relaxation time  $\tau$ . Here it is important to stress that the partial specification of boundaries in the case of mixed boundary conditions generically leads to multiple solutions which compete in establishing the local configurations of gates consistent with the global constraints defining the computational circuit. While we will come back to cases with multiple solutions and no solution in Sec. IIIB2, the focus of this paper is on problems with a single solution. To ensure a single solution in the case of mixed boundary conditions we always check that each of the random instances of the input state for a given circuit allows for one and only one solution.

Our results are represented in the form:

$$\ell(\tau) = \langle m \rangle(\tau) WL/L_\partial , \quad (17)$$

which defines a dynamical correlation length,  $\ell(\tau)$ . To motivate Eq. (17) we note that the domain of satisfied gates that contribute to  $\langle m \rangle(\tau)$ , the fraction of gates that reach their correct states at time  $\tau$ , grows from the pinned states at the boundaries, and covers an area  $L_\partial \times \ell(\tau)$ . Thus  $\ell(\tau)$  describes the growth of correlated regions of satisfied gates that eventually connect the two boundaries of the circuit.

In Fig. 4 we present the numerical results for the fixed input and output case and the mixed boundary conditions case as described above, with different concentrations of TOFFOLI gates. Remarkably, we find that the curves for different system sizes  $L$  and  $W$  collapse very well when scaled as in Eq. (17). In addition, notice that for shorter circuit with fixed input and output and low concentration of TOFFOLI gates (20%),  $\ell(\tau)$  begins to saturate for large enough  $\tau$  (Fig. 4a). As shown more clearly in Fig. 5a, this saturation occurs when the dynamical correlation length  $\ell(\tau)$  reaches  $W/2$ , where the growing domains of satisfied gates meet. Since in this case  $L_\partial = 2L$ ,  $\ell(\tau_s) \sim W/2$  corresponds to  $\langle m \rangle(\tau_s) = 1$  establishing  $\tau_s$  as the time-to-solution. For mixed bound-

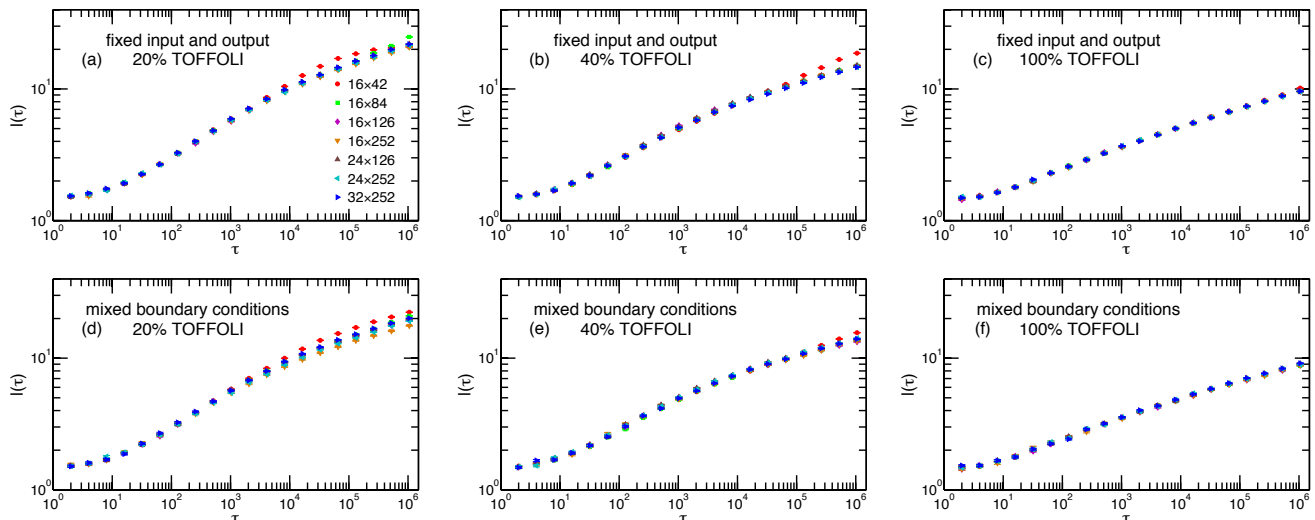


Figure 4. The average dynamical correlation length  $\ell(\tau)$  as a function of the annealing duration for different circuit sizes ( $L \times W$ ). For all sizes and cases, 2000 realizations of the boundary states were used. The data-point code used in panel (a) applies to all other panels. When not visible, the error bars are smaller than the size of the data points. (a)-(c) fixed input and output; (d)-(f) mixed boundary conditions; (a)&(d) 20% TOFFOLI; (b)&(e) 40% TOFFOLI; (c)&(f) 100% TOFFOLI. For systems with the smallest depth  $W$  studied,  $16 \times 42$ , and for circuits with few TOFFOLI gates (20%) and fixed input and output boundary conditions,  $\ell(\tau)$  tends to saturate, indicating that complete solutions have been reached. Notice that the functional form of the scaling does not depend on the boundary conditions, and depends solely on the concentration of TOFFOLI gates.

ary conditions, however,  $\ell(\tau) \sim W/2$  initiates the communication between the two boundaries and establishes the system’s capacity to “learn” (see below) but is not sufficient for negotiating solution. Indeed, Fig. 5a shows that  $\langle m \rangle(\tau)$  does not yet saturate when  $\ell(\tau) \sim W/2$ . As can be seen from Fig. 6 for computations with mixed boundary conditions, correlations must develop along the transverse direction (*i.e.*, parallel to the boundaries) before solution can be reached. In those cases it is this slower process that determines the time-to-solution and dominates the complexity of computations.

Finally, we discuss the effect of increasing the concentration of TOFFOLI gates that, as already alluded to above, reflect an increase in the complexity of the computation. In Fig. 5b, we show curves for the same system size with different concentrations of TOFFOLI gates. It is clear that correlations across the two boundaries grow more slowly as the concentration of TOFFOLI gates increases. The case of no TOFFOLI gates is equivalent to  $3L$  decoupled ferromagnetic Ising chains. In this case the dynamic correlation length behaves as  $\ell(\tau) = \ell_0[(\tau/\tau_0)/\ln(\tau/\tau_0)]^{1/2}$  (with  $\ell_0 = 1.42$  and  $\tau_0 = 8.33$ ) as illustrated by the dashed line in Fig. 5b. This behavior is in agreement with the exact result for the Kibble-Zurek dynamical scaling of the density of domain walls in a ferromagnetic Ising chain [36].

## 2. “Annealing with Learning”

In the previous sub-section we studied the evolution of solutions to the vertex model representations of computations described by different boundary conditions via thermal annealing and we identified a growing length scale  $\ell(\tau)$  that controls the communication between the two boundaries. There are a number of important conclusions reached on the basis of these thermal annealing simulations: Even in the case of forward computation the time-to-solution reached when the dynamic correlation length grows to  $\ell(\tau) \sim W/2$  is slower than ballistic as expected for deterministic forward computation. This can be already seen from the exactly solvable case with no TOFFOLI gates. Moreover, for single-solution problems with mixed boundary conditions the growth of correlations establishing communication between boundaries grow with the same scaling form as in direct computation (see Fig. 4). However, in that case negotiating solution requires the establishment of much slower correlations *along* the boundaries, a process for which a “vanilla” thermal annealing approach is extremely inefficient and would require unreasonably large computational resources.

These shortcomings are addressed by using a heuristic “learning” protocol in which annealing is carried out independently in  $N_R$  exact replicas of the vertex model and one assigns gate identities according to an appropriately chosen majority rule among replicas. Reaching solution involves repeating the “learning” process by ap-

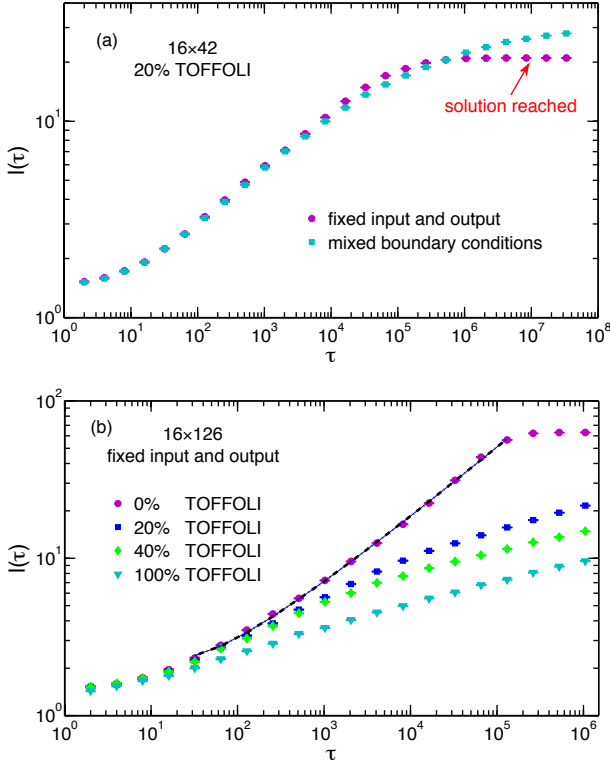


Figure 5. (a) The saturation of the scaling curve for fixed input and output boundary conditions with 20% TOFFOLI gates when  $\ell(\tau) \sim W/2$ . This indicates that the solutions have been reached, and is consistent with the domain growth picture. Notice that for mixed input and output boundary conditions, the curve does not saturate when  $\ell(\tau) \sim W/2$ . (b) The functional form of the scaling curves as a function of different TOFFOLI concentrations. The correlation grows more slowly as the concentration of TOFFOLI gates increases. The dashed line corresponds to the fitting  $\ell(\tau) = \ell_0[(\tau/\tau_0)/\ln(\tau/\tau_0)]^{1/2}$ , with  $\ell_0 = 1.42$  and  $\tau_0 = 8.33$ .

plying it to unassigned gates that failed to satisfy the replica majority rule in the previous iteration until all gates in the system are fixed. This approach leads to a dramatic speed-up of computations and, in particular, it translates into a time-to-solution for forward computations that scales linearly with  $W$ .

More precisely, the “annealing with learning” algorithm proceeds through the following steps: (1) one starts by annealing  $N_R$  identical replicas of a circuit over some time  $\tau_a$ , during which the correlation lengths grow beyond a few columns of gates such that the probability for assigning correct gates within that region,  $p \sim \exp -|x|/\xi > 1/2$ , within each replica; (2) one then assigns a specific identity to each gate (with  $p > 1/2$ )

provided that a fraction of the  $N_R$  replicas, greater than or equal to  $\alpha$ , agree on this assignment; (3) with the agreed upon gates frozen, the annealing process is independently applied again to each of the replicas allowing only gates not yet pinned to participate in the Metropolis algorithm; finally, (4) the procedure is iterated until all gates are fixed, thus establishing the solution to the problem.

This protocol raises the question of how many replicas  $N_{R\epsilon}$  are needed to ensure that the learning algorithm reaches the correct result with a probability greater than  $1 - \epsilon$ . In particular, how does  $N_{R\epsilon}$  depend on the system size  $L \times W$  and the threshold  $\alpha$ ? As we show in the Supplementary Information, the number of replicas needed to ensure an error rate smaller than  $\epsilon$  is given by  $N_{R\epsilon} = \frac{\ln[\frac{2p-1}{p} \frac{\epsilon}{LW}]}{\ln[2p^{1-\alpha}(1-p)^\alpha]}$ , where  $p > \frac{1}{2}$  is the probability of a correct gate assignment for one replica. Note that, for fixed  $\alpha$  and error rate  $\epsilon$ , the number of replicas grows only *logarithmically* with the system size, and thus in practice the learning algorithm works with reasonable resources.

Before describing the results of applying “annealing with learning” to computations with both fixed and mixed boundary conditions algorithm, in Fig. 6 we plot the average local overlaps of 2000 replicas with the solution for a fixed circuit and boundary condition before applying the learning algorithm. The agreement with the data presented in Sec. III B 1 substantiates the fact that the local majority rule implemented through the independent annealing of the replicas recapitulate the behavior of the correct solution to the computational problem.

*Fixed Boundary Conditions:* Using the algorithm described above, we choose  $\tau_a = 2^{13}$  for each iteration, and set the majority rule threshold at  $\alpha = 0.7$ . In Fig. 7 we show the local order parameter of the final states averaged over 2000 replicas after each iteration. We emphasize that even though we are plotting the average overlap with the actual solution as a benchmark, in the learning algorithm no reference to  $\{q^{sol}\}$  is made. The weight of each possible state of each gate in the circuit is computed solely from the replicas. After each iteration, with  $\tau_a = 2^{13}$  the correlation length grows to  $\ell(\tau_a) \sim 10$ , and by pinning gates with high percentage of agreement on certain states we are pushing the “boundary” forward until all gates are fixed. Since the total number of iterations  $n_a$  scales linearly with the circuit depth  $W$ ,  $n_a \propto W$ , the total time to solution  $\tau = n_a \tau_a$  also scales linearly with  $W$ ,  $\tau \propto W \tau_a$ , consistent with the expectations for the time-to-solution for forward computation. For the computation shown in Fig. 7, it is clear that the “annealing with learning” process proceeds ballistically and reaches solution with  $n_a = 9$  steps.

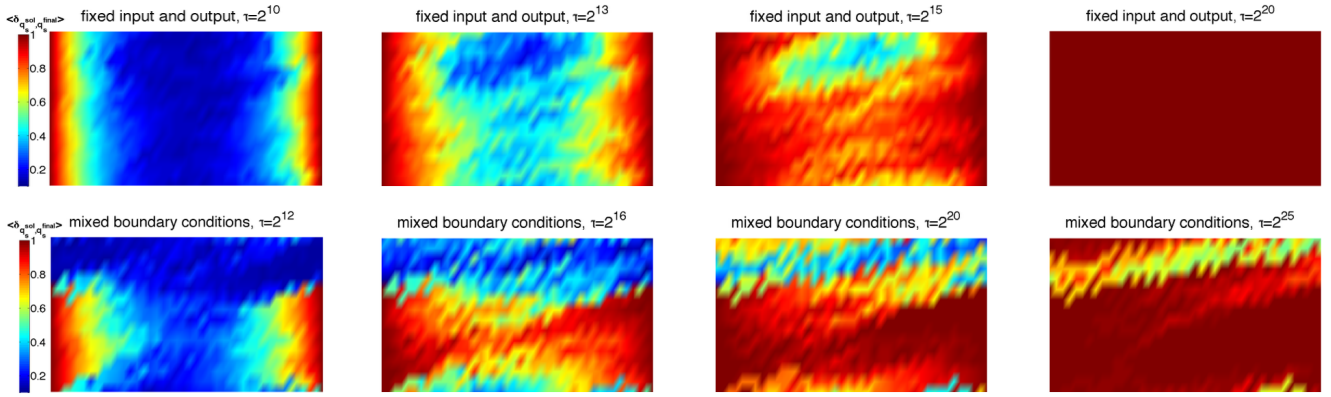


Figure 6. The average local overlaps  $\langle \delta_{q_s^{\text{sol}}, q_s^{\text{final}}} \rangle$  of 2000 replicas with  $\{q^{\text{sol}}\}$  for a given circuit and boundary state without learning. The system size is  $16 \times 42$ , with 20% TOFFOLI gates. Upper panel: fixed input and output; lower panel: mixed boundary conditions.

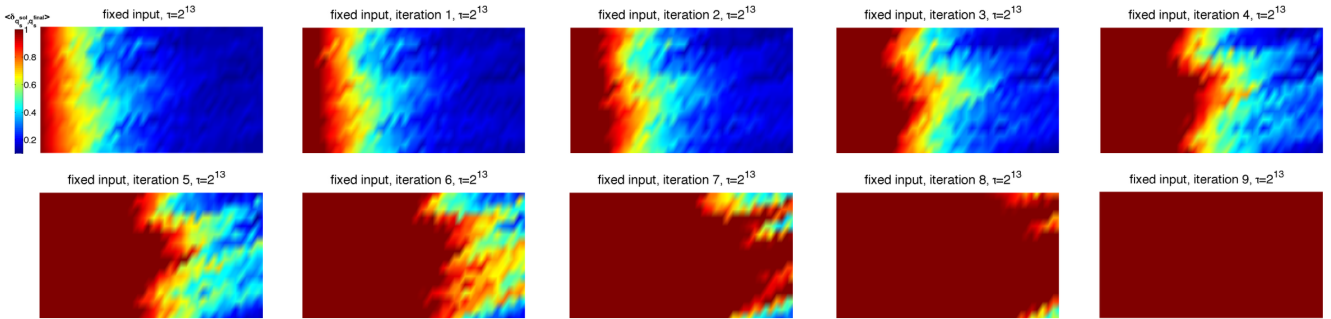


Figure 7. Annealing with learning for the fixed input boundary case for a system of size  $16 \times 42$  with 20% TOFFOLI gates. The annealing time within each iteration is  $\tau_a = 2^{13}$  and the gate state probability threshold  $\alpha = 0.7$ .

*Mixed Boundary Conditions:* The results presented in Fig. 8 are obtained by applying the learning algorithm with  $\alpha = 0.7$ . However, in the case of mixed boundary conditions the process of “learning” proceeds through two series of annealing steps with different time scales: an initial set of iterations with  $\tau_a = 2^{13}$  which build longitudinal correlations required for learning, followed by a set of longer annealing steps with  $\tau_b = 2^{18}$  that allow the slower correlations along the transverse direction to develop. Figure 8 shows the progression to solution, which could not be reached for the same computation using the “vanilla” thermal annealing for our longest accessible times ( $\tau \sim 2^{25}$ ).

We note that this protocol can also be used to solve problems with a “few”,  $\mathcal{O}(1)$ , solutions. This is best illustrated for the case of two solutions, which can be addressed by carrying out  $2n$  computations with mixed boundary conditions, where  $n$  is the number of unknown bits in the input. The idea is to define  $2n$  problems by fixing each bit at a time to be 0 or 1, while leaving the other  $n - 1$  bits floating. Since the two solutions must differ in at least one of the  $n$  bits, after at most  $2n$  steps,

this scheme transforms the problem into two separate problems, each of which can be solved by the techniques discussed in this paper. An important problem that falls precisely within this case is factorization of semi-prime numbers  $s = p \times q$ , where there are exactly two solutions, corresponding to the two ordered pairs  $(p, q)$  and  $(q, p)$  of primes  $p, q$  (assumed to be different).

Finally, we turn to the analysis of cases with multiple solutions and no solution. In both of these cases it is not sensible to compute the local overlap with a solution, as we did for circuit problems with only one solution. Instead, we plot the largest weight of each gate state in the circuit obtained from 2000 replicas. This is shown in Fig. 9 for an instance with 8 solutions obtained by fixing fewer gates (than in the single solution case) on each boundary; and an instance with no solutions, obtained by fixing a few gates on one boundary to the wrong states. Fig. 9 shows that the learning algorithm eventually gets stuck when the replicas cease to agree on gate assignments above the threshold  $\alpha$ . We note that the learning algorithm cannot differentiate between these two cases. We interpret the freezing of the system as an effect of

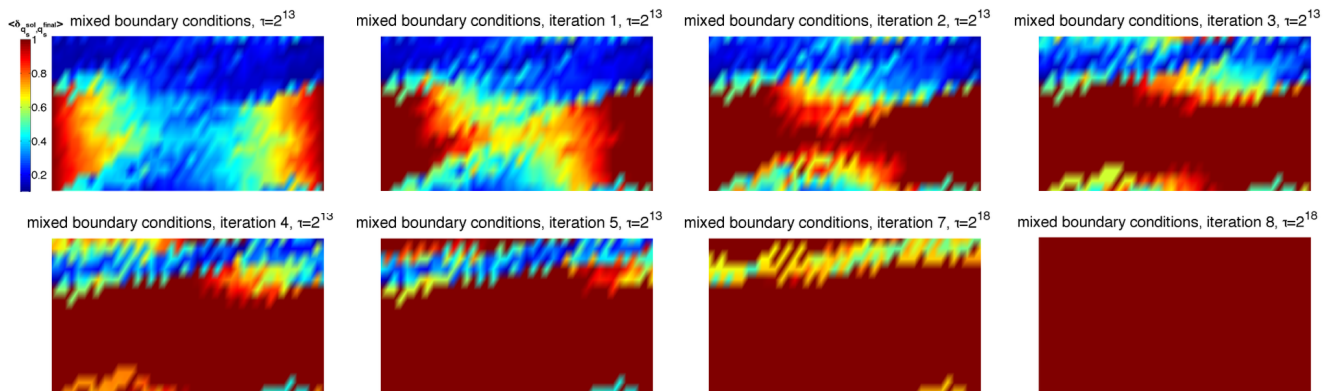


Figure 8. Annealing with learning for mixed boundary conditions and systems of size  $16 \times 42$  with 20% TOFFOLI gates. The annealing time within each iteration is  $\tau_a = 2^{13}$ , and the probability threshold  $\alpha = 0.7$ . After the correlations build up along the longitudinal direction,  $\tau_a$  is increased to  $\tau_b = 2^{18}$ .

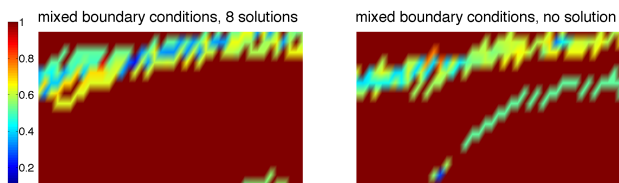


Figure 9. Color plot of the largest weight of each gate state in the circuit for a system of size  $16 \times 42$  and 20% TOFFOLI gates after a relaxation time  $\tau \approx 2^{20}$ . Left panel: case with 8 solutions; right panel: case with no solution. The learning algorithm eventually gets stuck at the point where no more gates have majority weight above the threshold  $\alpha$ .

frustration in satisfying the local gate constraints in the bulk induced by incompatible boundaries in the case of no solution or compatible but competing boundaries in the case of multiple solutions.

#### IV. QUANTUM ANNEALING AND THE MAPPING OF THE TILE MODEL ONTO THE D-WAVE CHIMERA GRAPH

In Sec. III we studied the thermodynamics and the dynamics of the vertex model in its classical limit,  $\delta = \Delta/K = 0$ . Thermal annealing, either its plain implementation or the combination of annealing and learning presented in Sec. IIIB2, can be part of a strategy for finding the solutions of computational problems embedded in ground state of the vertex model. In all of those discussions one could replace thermal by quantum annealing.

The solution of classical computation can be reached by starting in the ground state of the quantum Hamiltonian in Eq. (8) at large  $\delta$  and adiabatically decreasing  $\delta$  to zero. We argue that this path to the solution must encounter a zero-temperature quantum phase tran-

sition at a finite value of  $\delta$ . This follows from considering trivial classical circuits with no TOFFOLI gates in which case an  $L \times W$  vertex model is equivalent to  $3L$  decoupled Ising chains of size  $W$  in a transverse magnetic field. Just as in the one-dimensional Ising model in a transverse field, in the limit of no TOFFOLI gates one expects a zero temperature second-order quantum phase transition at  $\delta_c = 1$ . The addition of TOFFOLI gates complicates the analysis, but on physical grounds we expect that the phase transition cannot simply disappear, but change character, from second order to first order. This could happen if the no-TOFFOLI critical point happens to be an endpoint of a phase boundary in the  $\delta$ - $c$  plane, where  $c$  is the concentration of TOFFOLI gates. However, determining the order of the transition for the vertex model describing a generic computation is a difficult problem, which we expect to address via quantum Monte Carlo simulations in a future publication. The conjectured equilibrium phase diagram for the quantum vertex model is shown in Fig. 10.

With the goal in mind of utilizing quantum annealing as an alternative path to solution, in the remainder of this paper we describe a scheme for “programming” our vertex model into a quantum annealer. In particular, we present an explicit embedding of the tile model of universal classical computing circuits into the Chimera graph architecture of the D-Wave machine. The idea is to use one unit cell to represent one square tile of our construction presented in Sec. II A. Rectangular tiles (i.e., TOFFOLI gates) can be viewed as consisting of two square tiles, thus requiring two unit cells to be embedded in the Chimera graph. We then implement the Hamiltonians of Eqs. (1)-(3) using the programmable couplers available in the D-Wave machine.

Figure 11 shows the ‘flow chart’ of embedding a  $4 \times 4$  tile lattice into the Chimera graph. The entire tile lattice is rotated by  $45^\circ$  for convenience, and spins living on the boundary of each tile are shown explicitly. The lattice of tiles can be further divided into two sublattices

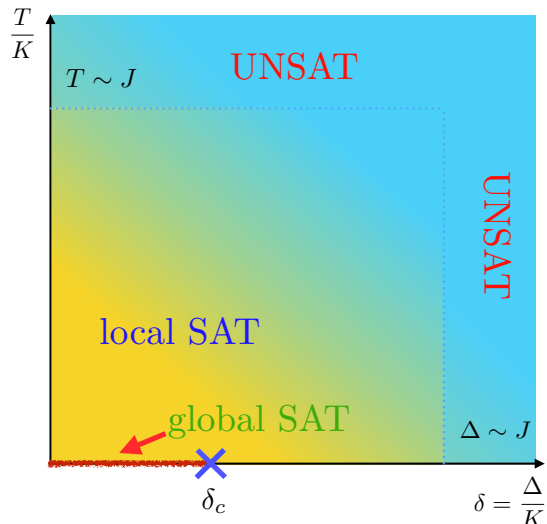


Figure 10. Phase diagram of the vertex model defined by Eq. (8). Our exact calculation of the partition function shows that there is no phase transition along the classical path ( $\delta = 0$ ). We argue that there should be a quantum phase transition for some critical  $\delta_c$ .

labeled by dark and light grey, for reasons that should become clear shortly. Now let us first consider how to encode the ID and SWAP gates represented by a single square tile into a unit cell. The embedding involves internal couplings  $J$  that enforce the gate constraints, and the “grout” couplings  $K$  that match adjacent tiles. The Chimera unit cell forms a complete bipartite graph  $K_{4,4}$ , as depicted in Fig. 11b-(i), with each spin in one column coupled to all spins in the other, but not to those in their own column [37]. In order to obtain the generic spin couplings to represent the gates on a single tile, which inevitably involves couplings between qubits in the same column as well, we use an additional ferromagnetic coupling to slave the spins in one column to their nearest neighbors in the other column. Thus, effectively we are left with four spins that are fully connected. Details are shown in Fig. 11b-(i).

In order to use the connectivity of the Chimera graph architecture and couple adjacent tiles properly, it is convenient to explore the bipartiteness of the square lattice. Let us take one tile from the rotated tile lattice, and label the four qubits by their locations on the tile: N (North), S (South), W (West) and E (East), as shown in Fig. 11b-(ii). The spins in the adjacent tiles are matched by the “grout” coupling  $K$ . Upon a careful inspection of the resulting tile lattice, we notice that the qubits labeled by N and W in one tile are always connected respectively to qubits S and E in its neighbor. Therefore, once we fix the embedding of one sublattice in the unit cell, the embedding of the other sublattice must be different, because qubits in one unit cell are only coupled to those at the same place in the neighboring unit cell. We map the two sublattices of the tile lattice in the unit cells as

illustrated in Fig. 11b-(ii).

Finally, let us show how to embed the TOFFOLI gate, which corresponds to a rectangular tile, into the unit cells. The TOFFOLI gate can be viewed as consisting of two square tiles, thus requiring two unit cells, and the spins coupled between these two tiles exactly provide the ancilla bit needed in Hamiltonian of Eq. (3). Similar to the square tiles considered above, within a unit cell we use additional ferromagnetic couplings to slave qubits from one column to the other when necessary. The explicit mapping is shown in Fig. 11b-(iii). As we have already seen, in order to come up with a proper embedding, one has to carefully take into account how qubits are coupled to adjacent unit cells. Putting all of the above ingredients together, we arrive at the embedding of the entire  $4 \times 4$  tile lattice including TOFFOLI into the Chimera graph, as shown in Fig. 11a.

## V. DISCUSSION

The results of this paper were motivated by an attempt to use our statistical mechanics intuition about lattice models of spin systems to uncover some of the salient features of universal classical reversible computation for which we construct an explicit mapping onto a new class of statistical mechanics vertex models. In this approach the solution of any classical computational problem is encoded in the ground state of a vertex model representation of the computational circuit with appropriate boundary conditions on inputs and outputs. There are questions posed and open problems raised by these studies. Here we list five of the ones we find most important.

1. One should understand the scaling of time-to-solution of the various schemes discussed here, including those that utilize learning, as a function of input size and depth for specific computational problems. Under a trivial reduction scheme, one can solve problems with two solutions using similar annealing with learning techniques that we deployed for problems with a unique solution. As an important application we are already investigating the problem of the factorization of semi-primes. The scaling properties of the time-to-solution in the context of this concrete and relevant problem should be contrasted to that obtained in the random circuit with the same concentration of TOFFOLI gates.

2. Another question raised by our work is the nature of the zero-temperature quantum phase transition encountered in the quantum vertex model, as depicted in Fig. 10. We demonstrated that, in the limit of the trivial computational circuit with no TOFFOLI gates, this transition is second order, in direct analogy to the case of the one-dimensional Ising model in a transverse magnetic field. Whether the transition remains second order or becomes first order for realistic computations (corresponding to a finite concentration of TOFFOLIs) has very important consequences for solutions of computational problems via

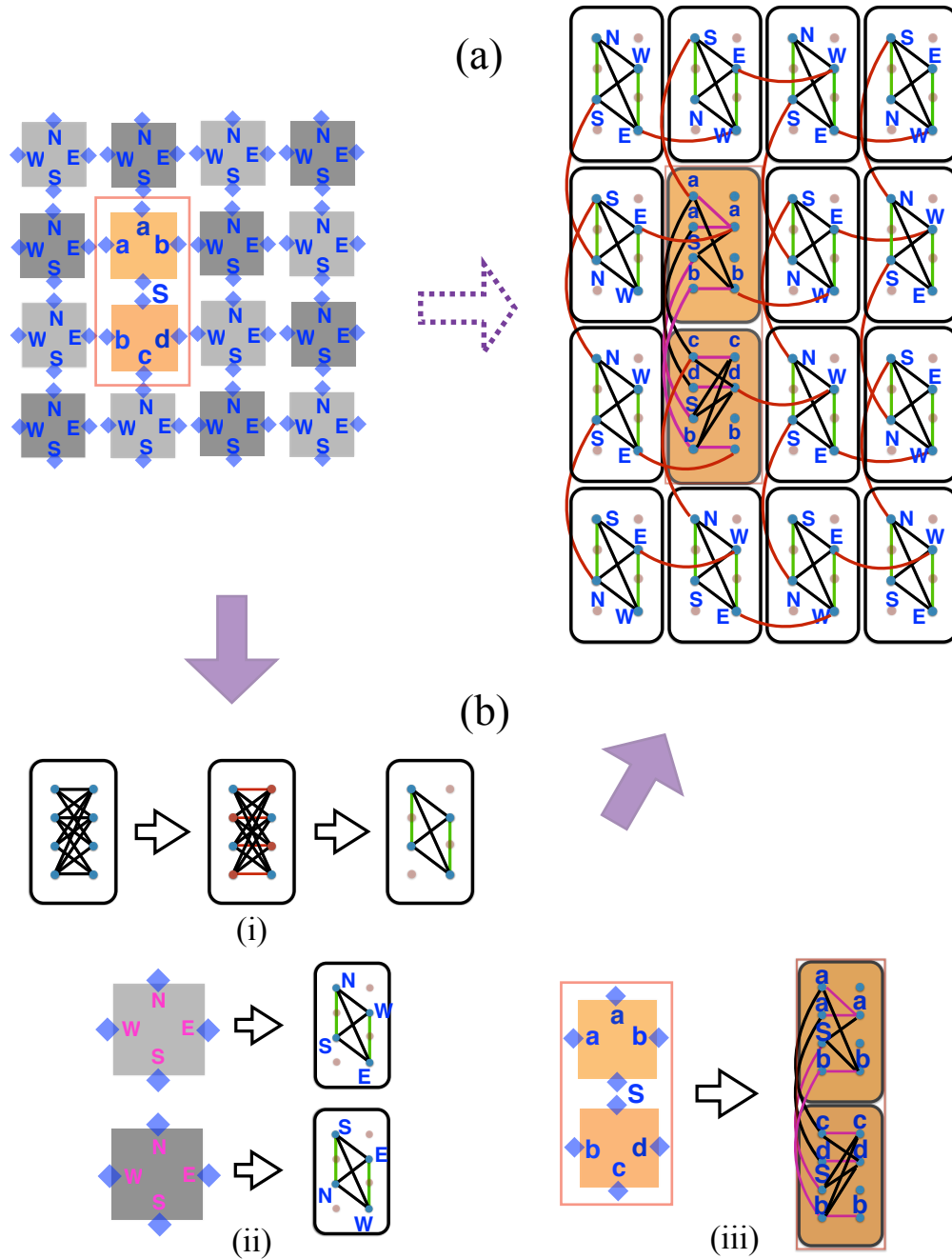


Figure 11. Procedure for embedding a  $4 \times 4$  tile lattice into the Chimera graph. (a) Left: a generic tile lattice rotated by  $45^\circ$ . Spins are put on the boundary of each tile. The lattice can be further divided into two sublattices, depicted by dark and light grey respectively; right: embedding of the tile lattice into the Chimera graph. The “grout couplings” are indicated by red links. (b) Embedding of each gate into the unit cells of the Chimera graph. (i) Left: a  $K_{4,4}$  unit cell of the Chimera graph; middle: in order to couple qubits in the same column, we slave the qubits to their neighbors in the other column using additional ferromagnetic couplings indicated by red links; right: effectively we are left with four qubits that are fully connected. For simplicity, we hereafter denote the effective couplings between spins in the same column by a single green link. However, one should keep in mind that they are obtained by slaving the spins to the opposite column via large ferromagnetic couplings. (ii) The four qubits in the rotated square tile are labeled by their locations on the tile: N (North), S (South), W (West) and E (East). Tiles corresponding to different sublattices must be embedded differently due to the special connectivity of the Chimera graph. (iii) Embedding of the TOFFOLI gate consisting of two square tiles into two unit cells.  $(a, b, c, d)$  corresponds to the input and output bits of the gate, and  $S$  is the ancilla bit. In the unit cell, ferromagnetic couplings that copy spins are indicated by purple links, and couplings required in Hamiltonian (3) are indicate by black links.

quantum annealing.

3. The computational problems discussed here should

also be studied directly in a *bona fide* quantum annealer. An important result of this paper is the programming of generic reversible computational circuits into the Chimera architecture of the D-Wave machine. This paves the way for using this type of hardware to study annealing protocols along the  $\delta$  axis, as well as arbitrary directions in the  $\delta - T$  plane.

4. In addition to exploring the mapping of the statistical mechanical model onto the Chimera architecture of the D-wave machine the approach presented in this paper should be used as a guide to the development of alternative machine architectures optimized for direct implementations of the vertex model.

5. Finally, we close with a brief discussion of the broader implications of the mapping of reversible classical computation onto the vertex model on the individual disciplines of computer science and physics. As already alluded to earlier the line of argumentation of this paper follows a physics perspective, namely it concentrates on “typical behavior” based on heuristic approach to explicit instantiations of the vertex model. Computer science could benefit from further work on more sophisticated theoretical and computational heuristic approaches, special purpose hardware (*i.e.*, quantum annealers), and new formal proofs that rely on statistical mechanics representations of computational problems. At the same time there are lessons to be learned from computer science that we believe may have interesting implications for physics. For example, if  $NP \neq P$ , the vertex model representing the hardest problems in UNIQUE-SAT can be also viewed as describing a physical glassy system that displays slow dynamics even though the model: (i) involves no frustrating interactions; (ii) has a unique non-degenerate ground state; and (iii) displays no bulk thermodynamic transitions down to zero temperature! There are known examples of systems with glassy dynamics in the absence of a thermodynamic phase transition, such as the kinetically constrained models discussed in [38–40]. However, the non-Arrhenius relaxation characteristic of these models only translate into a quasi-polynomial time-to-solution of a computational problem. Thus, within the vertex model approach, the existence of hard UNIQUE-SAT problems with exponential or sub-exponential behavior of the time-to-solution would suggest the existence of a novel family of glassy physical systems without a thermodynamic transition but with exponentially large barriers and corresponding astronomically-long relaxation times. This example underscores the richness of the possibilities opened by explorations of the vertex model of classical computation and more generally, of problems at the interface between physics and computer science.

## Appendix: Supplementary Information

### 1. Implementing the TOFFOLI gate with one-and two-body interactions

In this Appendix, we present the table with all possible configurations of a TOFFOLI gate formulated in a rectangular tile, and their corresponding energies given by Eq. (3). From which it is clear that the states which satisfy the gate constraint all stay in the ground state manifold of the Hamiltonian.

The TOFFOLI gate takes a three-bit input state  $(a, b, c)$  into  $(a, b, ab \oplus c)$ . The copying of the first two bits is trivially enforced by a ferromagnetic coupling:  $-J(\sigma_a \sigma_{a'} + \sigma_b \sigma_{b'})$ , so we shall only list the part that enforces the third output bit:  $d = ab \oplus c$  in the table below. As explained in Sec. II A, in order to achieve that with at most two-body interactions, one needs an ancilla bit that we call  $S$ .

In Table I, the first eight states separated by double lines span the ground state manifold of Hamiltonian (3), and one can readily check that they indeed satisfy the gate constraint imposed by the TOFFOLI gate. All other unsatisfying states have energy scales higher by multiple of  $J$ . Therefore in the limit where  $J$  is much larger than any other energy scale in the system ( $K, \Gamma$  and  $T$ ), one essentially projects out the ground state manifold. Notice that there are cases when  $(a, b, c, d)$  satisfies the gate constraint, but the ground state only picks one value of  $S$ . For example, the state  $(a, b, c, d) = (0, 0, 1, 1)$  satisfies the gate constraint, but the ground state manifold only picks  $S = 0$ , and  $S = 1$  has a higher energy. This does not cause a problem because the ancilla bit does not enter the computation, and its value does not really matter.

### 2. Nearest neighbor vertex couplings

The  $K_{q_s, q_{s'}}^{g_s, g_{s'}}$  couplings encode the energy cost for mismatched nearest-neighbor vertices. Here we give an example of how these matrix elements are constructed. Consider two adjacent vertices at  $s$  and  $s'$  that enforce the TOFFOLI gate:  $g_s = g_{s'} = \text{TOFFOLI}$  (or T for short). The matrix elements of  $K_{q_s, q_{s'}}^{T, T}$ , basically count the number of bits that are mismatched between the output state  $G(q_s)$  of one gate, where  $G$  is the gate function, and the input state  $q_{s'}$  of the other gate, for  $q_{s, s'} = 0, 1, \dots, 7$ .

When the two sites  $s$  and  $s'$  share a single bond, the

$a$	$b$	$c$	$d$	$S$	$\sigma_a$	$\sigma_b$	$\sigma_c$	$\sigma_d$	$\sigma_S$	$E$
0	0	0	0	0	-	-	-	-	-	$-13J$
0	0	1	1	0	-	-	+	+	-	$-13J$
0	1	0	0	1	-	+	-	-	+	$-13J$
0	1	1	1	1	-	+	+	+	+	$-13J$
1	0	0	0	0	+	-	-	-	-	$-13J$
1	0	1	1	0	+	-	+	+	-	$-13J$
1	1	0	1	0	+	+	-	+	-	$-13J$
1	1	1	0	1	+	+	+	-	+	$-13J$
0	0	0	1	0	-	-	-	+	-	$-9J$
0	0	1	0	1	-	-	+	-	+	$-9J$
0	1	0	1	0	-	+	-	+	-	$-9J$
0	1	1	0	1	-	+	+	-	+	$-9J$
1	0	1	0	0	+	-	+	-	-	$-9J$
1	1	0	0	0	+	+	-	-	-	$-9J$
1	1	0	0	1	+	+	-	-	+	$-9J$
1	1	1	1	0	+	+	+	+	-	$-9J$
1	1	1	1	1	+	+	+	+	+	$-9J$
0	0	1	0	0	-	-	+	-	-	$-J$
0	1	0	1	1	-	+	-	+	+	$-J$
1	0	0	1	0	+	-	-	+	-	$-J$
1	0	1	0	1	+	-	+	-	+	$-J$
0	0	0	0	1	-	-	-	-	+	$3J$
0	0	1	1	1	-	-	+	+	+	$3J$
0	1	0	0	0	-	+	-	-	-	$3J$
0	1	1	1	0	-	+	+	+	-	$3J$
1	1	0	1	1	+	+	-	+	+	$11J$
1	1	1	0	0	+	+	+	-	-	$11J$
1	0	0	0	1	+	-	-	-	+	$19J$
1	0	1	1	1	+	-	+	+	+	$19J$
0	0	0	1	1	-	-	-	+	+	$31J$
0	1	1	0	0	-	+	+	-	-	$31J$
1	0	0	1	1	+	-	-	+	+	$55J$

Table I. All possible configurations of a TOFFOLI gate formulated in a rectangular tile with an ancilla  $S$ , and their corresponding energies given by Eq. (3). The first eight states span the ground state manifold, and they satisfy the gate constraint.

$8 \times 8$  matrix  $K_{q_s, q_{s'}}^{T, T}$  (with  $q_{s, s'} = 0, 1, \dots, 7$ ) is given by

$$K^{T, T} = \begin{bmatrix} 0 & K & 0 & K & 0 & K & 0 & K \\ 0 & K & 0 & K & 0 & K & 0 & K \\ 0 & K & 0 & K & 0 & K & 0 & K \\ 0 & K & 0 & K & 0 & K & 0 & K \\ K & 0 & K & 0 & K & 0 & K & 0 \\ K & 0 & K & 0 & K & 0 & K & 0 \\ K & 0 & K & 0 & K & 0 & K & 0 \\ K & 0 & K & 0 & K & 0 & K & 0 \end{bmatrix}, \quad (\text{A.1})$$

and when the sites share a double bond, the  $8 \times 8$  matrix

is given by

$$K^{T, T} = \begin{bmatrix} 0 & 0 & K & K & K & K & 2K & 2K \\ K & K & 0 & 0 & 2K & 2K & K & K \\ K & K & 2K & 2K & 0 & 0 & K & K \\ 2K & 2K & K & K & K & K & 0 & 0 \\ 0 & 0 & K & K & K & K & 2K & 2K \\ K & K & 0 & 0 & 2K & 2K & K & K \\ 2K & 2K & K & K & K & K & 0 & 0 \\ K & K & 2K & 2K & 0 & 0 & K & K \end{bmatrix}, \quad (\text{A.2})$$

where  $K$  is the ferromagnetic energy scale that penalizes configurations in which the states of adjacent vertices are incompatible.

### 3. Bounds on Learning with Replicas

Below we estimate the number of replicas,  $N_R$  required to achieve the correct assignment of gates in the "annealing with learning" algorithm described in Sec. III B 2 with accuracy  $\epsilon$ . Assume that the probability of correct assignment of a gate within each replica is  $p$ . The probability that  $k$  of the  $N_R$  replicas assign the wrong identity to a given gate is given by the binomial distribution:

$$P(N_R, k; p) = \frac{N_R!}{(N_R - k)!k!} p^{N_R - k} (1 - p)^k. \quad (\text{A.3})$$

The probability that a fraction greater than  $\alpha$  of the  $N_R$  replicas ( $N_R \gg 1$ ) assign the wrong identity to a particular gate can then be written as:

$$\begin{aligned} P_w(N_R, \alpha; p) &= \sum_{k=\alpha N_R}^{N_R} \frac{N_R!}{(N_R - k)!k!} p^{N_R - k} (1 - p)^k \\ &< \frac{N_R!}{\left(\frac{N_R!}{2}\right)^2} \sum_{k=\alpha N_R}^{N_R} p^{N_R - k} (1 - p)^k \\ &\approx \frac{[2p^{1-\alpha}(1-p)^\alpha]^{N_R}}{\frac{(2p-1)}{p}}. \end{aligned} \quad (\text{A.4})$$

It then follows that, for fixed  $p > 1/2$ ,  $N_R$  and  $\alpha$ , the probability that a correct assignment is made to all  $LW$  gates by a fraction of the replicas greater than  $\alpha$  is  $1 - \epsilon$  is given by:

$$\begin{aligned} P_c(N_R, \alpha; p) &= [1 - P_w(N_R, \alpha; p)]^{LW} \\ &= 1 - \epsilon \\ &> 1 - LW \frac{[2p^{1-\alpha}(1-p)^\alpha]^{N_R}}{\frac{(2p-1)}{p}}, \end{aligned} \quad (\text{A.5})$$

which implies that the number of replicas,  $N_{R\epsilon}$ , needed to ensure an error rate smaller than  $\epsilon$  is given by:

$$N_{R\epsilon} = \frac{\ln \left[ \frac{2p-1}{p} \frac{\epsilon}{LW} \right]}{\ln [2p^{1-\alpha}(1-p)^\alpha]}. \quad (\text{A.6})$$

We note that the above argument assumes that the states of the gates are uncorrelated; for a given  $N_R$  the correla-

tions built into the vertex model should lead to a lower error rate than the estimate given here.

- 
- [1] M. Mézard and A. Montanari, *Information, Physics, and Computation* (Oxford University, Oxford, 2009).
- [2] M. Mézard, G. Parisi, and R. Zecchina, *Analytic and algorithmic solution of random satisfiability problems*, *Science* **297**, 812 (2002).
- [3] S. Ganguli and H. Sompolinsky, *Compressed sensing, sparsity, and dimensionality in neuronal information processing and data analysis*, *Ann. Rev. Neuroscience* **35**, 485 (2012).
- [4] P. Mehta and D. J. Schwab, *An exact mapping between the variational renormalization group and deep learning*, arXiv: 1410.3831 (2014).
- [5] R. Landauer, *Irreversibility and heat generation in the computing process*, *IBM J. Res. Dev.* **5**(3), 183 (1961).
- [6] R. Landauer, *The physical nature of information*, *Phys. Lett. A* **217**, 188 (1996).
- [7] C. H. Bennett, *The thermodynamics of computation—a review*, *Int. J. Theor. Phys.* **21**(12), 905 (1982).
- [8] M. A. Nielsen and I. L. Chuang, *Quantum Computation and Quantum Information* (Cambridge University Press, Cambridge 2000).
- [9] T. D. Ladd, F. Jelezko, R. Laflamme, Y. Nakamura, C. Monroe, and J. L. O’Brien, *Quantum computers*, *Nature (London)* **464**, 45 (2010).
- [10] A. R. Calderbank and P. W. Shor, *Good quantum error-correcting codes exist*, *Phys. Rev. A* **54**, 1098 (1996).
- [11] A. M. Steane, *Error correcting codes in quantum theory*, *Phys. Rev. Lett.* **77**, 793 (1997).
- [12] D. Gottesman, *Theory of fault-tolerant quantum computation*, *Phys. Rev. A* **57**, 127 (1998).
- [13] E. Knill, R. Laflamme, and W. H. Zurek, *Resilient quantum computation*, *Science* **279**, 342 (1998).
- [14] D. A. Lidar, I. L. Chuang, and K. B. Whaley, *Decoherence-free subspaces for quantum computation*, *Phys. Rev. Lett.* **81**, 2594 (1998).
- [15] D-Wave Systems Inc., <http://www.dwavesys.com>.
- [16] R. P. Feynman, *Quantum mechanical computers*, *Found. Phys.* **16**, 507 (1986).
- [17] J. D. Biamonte, *Nonperturbative k-body to two-body commuting conversion Hamiltonians and embedding problem instances into Ising spins*, *Phys. Rev. A* **77**, 052331 (2008).
- [18] I. J. Crosson, D. Bacon, and K. R. Brown, *Making classical ground-state spin computing fault-tolerant*, *Phys. Rev. E* **82**, 031106 (2010).
- [19] D. Whitfield, M. Faccin and J. D. Biamonte, *Ground-state spin logic*, *Eur. Phys. Lett.* **99**, 57004 (2012).
- [20] F. Ricci-Tersenghi, *Being glassy without being hard to solve*, *Science* **330**, 6011 (2010).
- [21] L. G. Valiant, and V. V. Vazirani, *NP is as easy as detecting unique solutions*, *Theor. Comp. Sci.* **47**: 85-93 (1986).
- [22] M. R. Garey and D. S. Johnson, *Computers and Intractability: A Guide to the Theory of NP-Completeness* (Freeman, New York, 1979).
- [23] C. H. Papadimitriou and K. Steiglitz, *Combinatorial Optimization – Algorithms and Complexity* (Dover, Mineola, NY, 1998).
- [24] S. Arora and B. Barak, *Computational Complexity: a Modern Approach* (Cambridge University, New York, 2009).
- [25] S. Kirkpatrick, C. D. Gelatt Jr., and M. P. Vecchi, *Optimization by simulated annealing*, *Science* **220**, 671 (1983).
- [26] B. Apolloni, C. Carvalho, and D. de Falco, *Quantum stochastic optimization*, *Stochastic Process Appl.* **33**, 233 (1989).
- [27] A. Finnila, M. Gomez, C. Sebenik, C. Stenson, and J. Doll, *Quantum annealing: a new method for minimizing multidimensional functions*, *Chem. Phys. Lett.* **219**, 343 (1990).
- [28] T. Kadowaki and H. Nishimori, *Quantum annealing in the transverse Ising model*, *Phys. Rev. E* **58**, 5355 (1998).
- [29] E. Farhi, J. Goldstone, S. Gutmann, J. Laplan, A. Lundgren, and D. Preda, *A quantum adiabatic evolution algorithm applied to random instances of an NP-complete problem*, *Science* **292**, 472 (2001).
- [30] V. Vedral, A. Barenco, and A. Ekert, *Quantum networks for elementary arithmetic operations*, *Phys. Rev. A* **54**, 147 (1996).
- [31] C. Castelnovo, C. Chamon, C. Mudry, and P. Pujol, *High-temperature criticality in strongly constrained quantum systems*, *Phys. Rev. B* **73**, 144411 (2006).
- [32] C.-W. Liu, A. Polkovnikov, and A. W. Sandvik, *Dynamic scaling at classical phase transitions approached through nonequilibrium quenching*, *Phys. Rev. B* **89**, 054307 (2014).
- [33] T. W. B. Kibble, *Topology of cosmic domains and strings*, *J. Phys. A: Math. Gen.* **9**, 1378 (1976).
- [34] W. H. Zurek, *Cosmological experiments in superfluid helium?*, *Nature (London)* **317**, 505 (1985).
- [35] S. Rubin, N. Xu, and A. W. Sandvik, *Dual time scales in simulated annealing of a two-dimensional Ising spin glass*, arXiv:1609.09024.
- [36] P. L. Krapivsky, *Slow Cooling of an Ising Ferromagnet*, *J. Stat. Mech.* P02014 (2010)
- [37] V. Choi, *Minor-embedding in adiabatic quantum computation: II. Minor-universal graph design*, *Q. Inf. Process.* **10**, 343 (2011).
- [38] M. E. J. Newman, and C. Moore, *Glassy dynamics and aging in an exactly solvable spin model*, *Phys. Rev. E* **60**, 5068 (1999).
- [39] J. P. Garrahan and M. E. J. Newman, *Glassiness and constrained dynamics of a short-range nondisordered spin model*, *Phys. Rev. E* **62**, 7670 (2000).
- [40] For a review, see F. Ritort and P. Sollich, *Glassy dynamics of kinetically constraint models*, *Adv. Phys.* **52**, 219 (2003).